CORB Origins:
Paleoceanographic and Paleoclimate Implications

ORIGIN OF CRETACEOUS OCEANIC RED BEDS FROM THE VISPI QUARRY SECTION, CENTRAL ITALY: VISIBLE REFLECTANCE AND INORGANIC GEOCHEMISTRY

XIUMIAN HU
State Key Laboratory of Mineral Deposit Research, Department of Earth Sciences, Nanjing University, Nanjing 210093, P.R. China
e-mail: huxm@nju.edu.cn
WENBIN CHENG
College of Earth Sciences, China University of Geosciences, Beijing 100083, P.R. China
e-mail: haitianyisu@126.com
AND
JUNFENG JI
Department of Earth Sciences, Nanjing University, Nanjing 210093, P.R. China
e-mail: jijunfeng@nju.edu.cn

Abstract: A major change in oceanic sedimentation from Uppermost Cenomanian organic-carbon-enriched black shales (Bonarelli Level) to predominantly Lower Turonian oceanic red beds occurred in the Tethys. This paper presents high-resolution inorganic geochemical and mineralogical data on the transitional interval from the Scaglia Bianca to the Scaglia Rossa above the Bonarelli Level of the Vispi Quarry section, Umbria–Marche basin, Italy. Limestones from the Vispi Quarry section have very low Al_2O_3 concentrations (0.19–1.14 wt%) indicating low input of terrigenous detritus. Elements characterizing lithogenic input, such as Ti, K, Mg, Rb, and Zr, are of similar concentration in both the white limestone and the red/pink limestone and correlate positively with Al_2O_3, pointing to a homogeneous source area. The sources of terrigenous detrital input did not change throughout the transition from the Scaglia Bianica to the Scaglia Rossa. Geochemical data show that the red limestones were deposited under more oxic conditions, close to the sediment–water interface, as opposed to the white limestones in the Vispi Quarry section. This is supported by: (1) high Fe_2O_3 values (0.22% in average) and high Fe^{3+}/TFe ratio (0.58); (2) low values of relative enrichment factor (EF) of redox-sensitive elements U, V, Cr, Co, and Ni in the red limestones, with ratios of Ni/Co < 2.5, V/Cr < 1.2, V/(V+Ni) < 0.6, Fe^{3+}/TFe > 0.45; and (3) a strongly negative δCe anomaly (0.28–0.42). The positive correlation between the peak height of hematite in the diffuse reflectance spectrophotometry (DRS) diagram and redness values ($R^2 = 0.98$) indicates that hematite is responsible for the color of the limestones in the Vispi Quarry section. The DRS data confirm that the red color of the Scaglia Rossa limestones is the result of low concentration (~ 0.1 wt%) of finely dispersed hematite. $SiO_{2(excess)}$, P, and Ba productivity proxies show that there is no significant difference in depositional conditions and paleoproductivity levels between red limestone and white limestone. An increase in dissolved oxygen in bottom waters is the most probable cause of the origin of the red color. We suggest that intensification of bottom circulation with waters having higher content of dissolved oxygen may have resulted in significant oxidation of bottom sediments.

Key words: CORBs, visible reflectance, inorganic geochemistry, major elements, trace elements, rare earth elements, hematite, Vispi Quarry section, Gubbio, Italy

INTRODUCTION

A major change in oceanic sedimentation from mid-Cretaceous organic-carbon-enriched deep-sea deposits to predominantly Upper Cretaceous oceanic red beds (CORBs), represented mainly by deep-sea red shales and marls, occurred during the Late Cretaceous and the Paleogene in the western Tethys (Hu et al., 2005; Hu et al., 2006a; Hu et al., 2006b; Melinte and Jipa, 2005; Wagreich and Krenmayr, 2005). Mid-Cretaceous black shales and associated oceanic anoxic events (OAEs) have been the subject of many studies during the past thirty years, since the pioneer study by Schlanger and Jenkyns (1976). Recently, two IGCP projects (IGCP 463/494), initiated in 2002 and 2003, respectively, have improved our understanding of the origin of CORBs and their ability to document paleoclimate, organic-carbon burial, and paleoceanography (Hu et al., 2005; Hu et al., 2006a; Wang and Hu, 2005). CORBs are found in a broad geographic belt extending from the North Atlantic, Spain, Italy, the Alps, the Carpathians, the Black Sea, the Caucasus, the Himalayas, to the western Pacific (Hu et al., 2005). CORBs are of pelagic and hemipelagic origin and were deposited in a variety of environments from continental slope to deep oceanic basins, above and below the carbonate compensation depth (CCD) (Hu et al., 2005; Hu et al., 2006a; Kuhnt and Holbourn, 2005; Wagreich and Krenmayr, 2005; Wang et al., 2005).

The transition and environmental change from black shales to red-bed facies in the aftermath of the latest Cenomanian Bonarelli black shales (OAE2) is less well studied. During this time interval in the latest Cenomanian to the Early Turonian, organic-carbon-enriched "black shale" facies was replaced by pelagic red beds. In the Umbria–Marche basin in central Italy (Fig. 1), eight pinkish, reddish, or maroon bands and zones in the Marne a Fucoidi and Scaglia facies occur in the interval from the Selli Level (OAE1a) to the Bonarelli Level (OAE2), which suggests variability in paleoceanographic conditions and perhaps indirectly in paleoclimate (Hu et al., 2006a). This paper concentrates on the transition from the OAE2 (Bonarelli Level) to the reddish-colored pelagic red beds of the Scaglia Rossa, cropping out in the Umbria–Marche Basin (Fig. 1). We present high-resolution inorganic geochemical and mineralogical data on the transitional interval from the

Cretaceous Oceanic Red Beds: Stratigraphy, Composition, Origins, and Paleoceanographic and Paleoclimatic Significance
SEPM Special Publication No. 91, Copyright © 2009
SEPM (Society for Sedimentary Geology), ISBN 978-1-56576-135-3, p. 183–197.

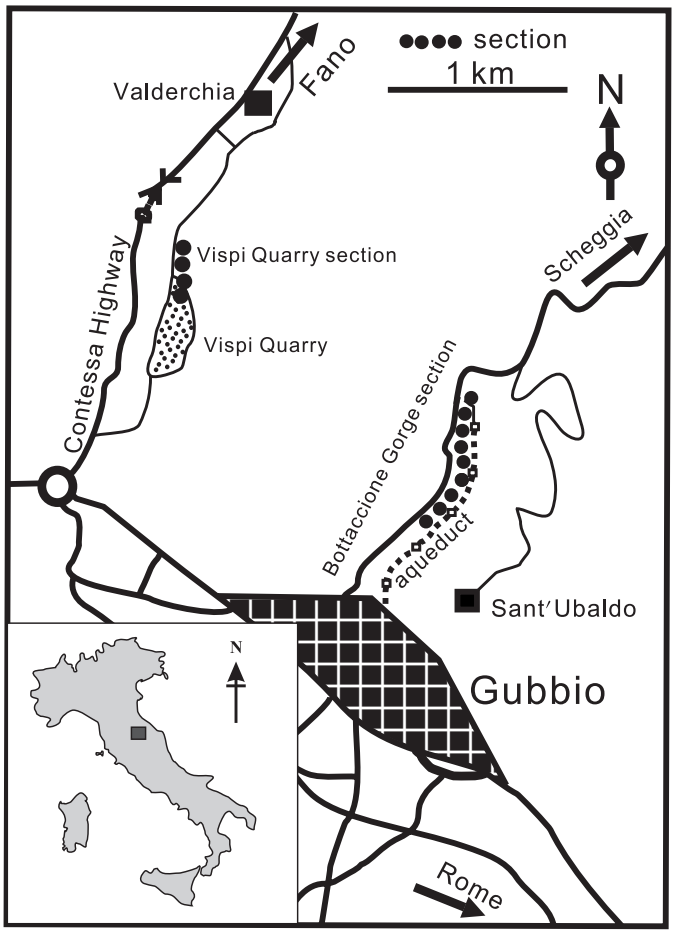

FIG. 1.—Location of the investigated section in the Vispi Quarry and the reference section of the Bottaccione Gorge near Gubbio, central Italy (revised from Montanari and Koeberl, 2000)

Scaglia Bianca to the Scaglia Rossa, on the basis of data from the Vispi Quarry section.

In this study, we employ the method of diffuse reflectance spectrophotometry (DRS) to study iron oxides and oxyhydroxides. Reflectance spectrophotometry transforms color to a quantitative measurement. Reflectance spectra are controlled by features related to electronic and vibration processes associated with the composition and structure of the material being analyzed. Many minerals exhibit diagnostic features in their near-ultraviolet (NUV), visible (VIS), and near-infrared (NIR) spectra (Balsam and Deaton, 1996). Reflectance spectrophotometry is especially sensitive to iron oxide and oxyhydroxide minerals, which are responsible for color variations in both marine sediments and continental red beds (e.g., Torrent and Schwertmann, 1987; Ji et al., 2001). However, little progress has been made yet in characterizing iron oxide concentrations in red beds, which probably results from the difficulty in identifying these minerals with standard techniques, such as X-ray diffraction (XRD). As demonstrated by Deaton and Balsam (1991), DRS has a detection limit for iron oxides as low as 0.03%, which is at least an order of magnitude lower than using XRD, for which the detection limit lies at 0.2%.

The purpose of this paper is three-fold: (1) to obtain information using inorganic geochemistry about the origin of the sediments, the oxygenation level of the water column, and paleoproductivity; (2) to compare the inorganic geochemistry of the red limestones to that of the white limestones in order to determine why the change between these two groups of sediments occurred; and (3) using DRS data to discuss iron oxide minerals which are responsible for the color of the CORBs. In the interpretation of the data we focus on paleoceanographic conditions indicated by geochemical and mineralogical data, with implications for the origin of CORBs.

SAMPLES AND METHODS

We studied sediments from the Vispi Quarry section (Fig. 1), cropping out on the eastern slope of the Contessa Valley about 2 km west of the town of Gubbio, and prepared a detailed stratigraphic log from the Bonarelli Level to the Scaglia Rossa of the Vispi Quarry section (Hu et al., 2006a). Here we use the biostratigraphy of the nearby Bottaccione Gorge section (Premoli Sliva and Sliter, 1994; Tremolada, 2002) (Fig. 1). In the Vispi Quarry outcrop, the white limestones of the Scaglia Bianca about 4.3 m above the Bonarelli Level grade into a sequence of predominantly pinkish-reddish limestones and marls—the Scaglia Rossa Formation (Fig. 2). Before the limestone succession becomes completely reddish, two transitional beds (the first at 10.35–10.55 m and the second at 10.63–10.83 m) occur (Fig. 2). Both transitional beds are of whitish color at the base with gradually increasing pinkish color towards the top. Above these two transitional beds, the limestone is fully pinkish, to reddish above 10.83 m (Fig. 2).

We analyzed samples from the Vispi Quarry using the DRS method to determine the minerals causing the color change. Sample preparation and analysis followed procedures described in Balsam and Deaton (1991) and Ji et al. (2002). Samples were ground to < 38 μm to thoroughly disperse all minerals, and spectral slides were prepared. Ground samples were suspended in distilled water to produce a slurry on a glass microslide, which was smoothed, dried slowly at low temperature (< 40° C), and analyzed in a Perkin-Elmer Lambda 6 spectrophotometer with a diffuse reflectance attachment (reflectance sphere) from 400 to 2500 nm at the Institute of Surficial Geochemistry at Nanjing University. Data processing was restricted to the VIS (400–700 nm), the region of the spectrum most sensitive to the occurrence of iron oxide minerals, which is responsible for the color variability (Deaton and Balsam, 1991). Data are given as percent reflectance relative to the Spectralon@ standard. Reflectance data converted into percent reflectance in standard color bands (Judd and Wyszecki, 1975), i.e., violet = 400–450 nm, blue = 450–490 nm, green = 490–560 nm, yellow = 560–590 nm, orange = 590–630 nm, red = 630–700 nm. Percent reflectance in each color band was normalized by the total visible wavelength reflectance in the sample. Percent-reflectance data were used to calculate sample brightness, that is, the area under the spectral curve. First-derivative values (percent per nanometer) were calculated at 10 nm intervals to enhance the variability of the reflectance data. The first-derivative transformation changes smooth-percent reflectance curves to curves with peaks where slopes change. Peaks in the first-derivative curves are indicative of a variety of minerals, especially iron oxides (Deaton and Balsam, 1991) and clay minerals (Balsam and Deatan, 1996).

In addition, we analyzed major-element, trace-element, and rare-earth-element concentrations in the red and white limestones adjacent to the transitional beds from 9.9 m to 11 m above the top of the Bonarelli Level (Appendix 1). Major-oxide analyses of the limestones were performed using X-ray fluorescence spectrometry (XRF). The loss on ignition (LOI) was determined by placing ~ 1 g of powdered sample into a weighed porcelain crucible and combusting in a furnace at ~ 1000° C for 4 hours. After cooling, samples were re-weighed and LOI was calculated

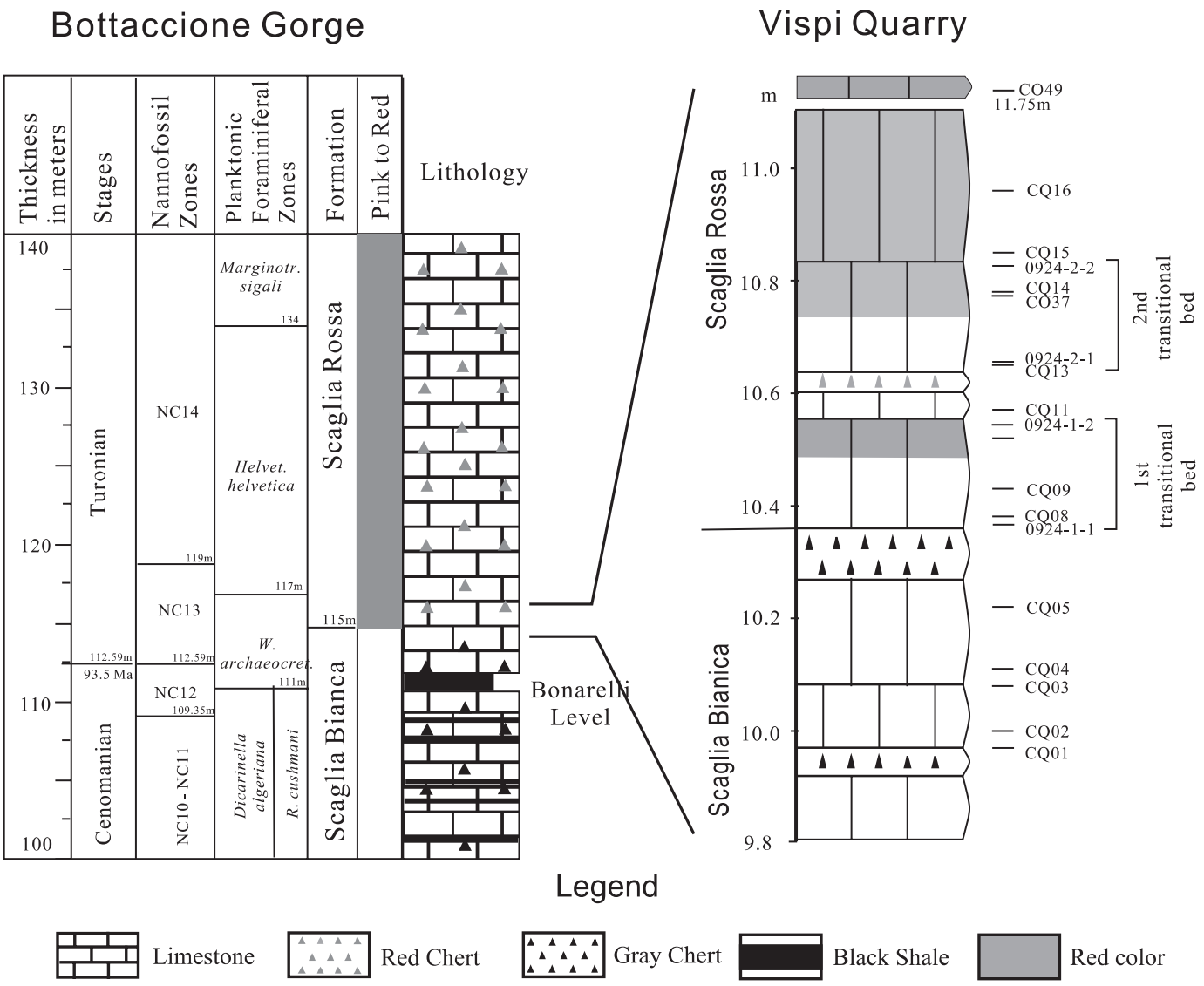

FIG. 2.—Detailed lithologic column from the Scaglia Bianca to Scaglia Rossa in the Vispi Quarry section, showing sample positions (right). Left: stratigraphic column from the Upper Cenomanian to the Turonian of the reference Bottaccione Gorge section, showing nannofossil and planktic foraminiferal zones (Premoli Silva and Sliter, 1994; Tremolada, 2002).

from the difference between pre- and post-combustion weights. Samples for XRF analysis were prepared by fusing 0.06 g of sample with 0.6 g of silica powder and 7.26 g of lithium borate ($Li_2B_4O_7$:$LiBO_2$ = 67:33) in a platinum crucible. The fused disks were then analyzed at the Nanjing University using a 9800XP+ X-ray fluorescence spectrometer. The analytical precisions for the oxides are estimated to be < 5%. Fe^{2+} (FeO) and Fe^{3+} (Fe_2O_3) were analyzed separately using a method by Wilson (1960).

The abundances of selected trace elements and rare earth elements were analyzed by ICP-MS (Appendix 1). Samples were dissolved in concentrated HF and HNO_3 (2:1 in volume) in tightly screwed Teflon beakers. After dissolution, 1 ml of concentrated HNO_3 was added to the solutions and dried twice to get rid of the HF in the samples. The sample solutions were finally dissolved in 2 ml of concentrated HNO_3, and spiked with 10 ppb Rh, and made up to 50 ml in 5% HNO_3 solution. These solutions were then measured using a Finnegan HR-ICP-MS at the State Key Laboratory for Mineral Deposits Research, Nanjing University. The analytical precision of trace elements and rare earth elements is better than 10%.

Elemental values were normalized to Al in order to account for dilution effects by potential biogenic components such as carbonates, silica, and phosphorites. Concentrations are compared to the average values of whole Vispi Quarry section and expressed as relative enrichments factors ($EF_{Element}$). Enrichment factors were calculated using: $EF_{Element} = (element/Al)_{Sample} \div (element/Al)_{section}$. Hence an element with the same Al-normalized ratio as the section would yield an EF of 1. Based on the elemental concentrations within the sediments, we use the term "enrichment" for $EF_{Element} \geq 1.2$, and we consider the samples "depleted" when $EF_{Element} \leq 0.8$. Given correlation problems associated with using normalized data in some cases (Van der Weijden, 2002), we also present and interpret some unmodified data.

RESULTS

DRS Data

As documented by Deaton and Balsam (1991), hematite and goethite can easily be identified in the first-derivative curves of DRS. Hematite is associated with a single prominent peak, either at 565 or 575 nm, and goethite has two first-derivative peaks, of which the primary peak is at 535 nm with a secondary peak at 435 nm (Balsam and Deaton, 1991; Deaton and Balsam, 1991). Both hematite and goethite peak heights increase as the percentage of the mineral increases (Deaton and Balsam, 1991, their Fig. 2).

Red and pink limestones in the Vispi Quarry section contain hematite, on the basis of DRS data from twenty samples, with a single prominent peak between 560 and 570 nm in the first-derivative curves (Fig. 3A). White limestones from the Vispi Quarry section lack both hematite and goethite because neither the hematite peak nor the two peaks of goethite are present (Fig. 3B).

In this paper we use the terminology of Balsam et al. (1999) to describe variations in light reflected from a sample surface. Optical lightness, or lightness, defines the amount of light reflected from a surface. Brightness is the area under the visible region of the spectral curve relative to a white standard. Brightness is increasingly used as a proxy for the carbonate content of marine sediment, where the composition of the noncarbonate sediment fractions has not changed significantly (Balsam and Deaton, 1996; Balsam et al., 1999). In the Vispi Quarry section, brightness varies from 66.9% to 93% with an average of 84.5% related to the white standard. The poor correlation between carbonate concentration and brightness in the Vispi Quarry section ($R^2 = 0.001$) show that brightness measures could not be directly used as a proxy for carbonate content in the pelagic limestones of the Scaglia facies.

Sediment color can be quantified by the percent reflectance in the red color band. Redness in sediment is related mainly to concentrations of iron oxide minerals, especially hematite and goethite (Ji et al., 2002). First-derivative analysis of the spectral data permits a mineralogical interpretation of iron oxide minerals at low concentrations (Deaton and Balsam, 1991). The comparison of first-derivative curves of samples with different redness values clearly illustrates that hematite is the main iron oxide responsible for the red color in the Scaglia Rossa limestones (Fig. 3A). The height of the hematite peak increases at increased redness values. As stated by Deaton and Balsam (1991), the height of hematite can be used as a proxy for hematite concentrations. Redness values vary from 23.5% to 27.2% in the Vispi Quarry section. Redness of red/pink limestones (24.1%–27.3% with an average of 25.0%) is higher than that of white limestones (23.5%–23.8% with an average of 23.6%). The positive correlation between the peak height of hematite and redness values ($R^2 = 0.98$) indicates that hematite concentration controlled not only the hue of the red color but also the deepness of the red color of the limestones in the Vispi Quarry section (Fig. 4).

Major Elements

The limestone samples studied are composed mainly of $CaCO_3$ (91.06–97.22 wt %) (Fig. 4) as calculated from the CaO values using an oxide conversion factor of 1.7751. Other major elements are present in low concentrations, owing in part to a dilution effect of carbonate (Table 1). In comparison with the white limestones, the red limestones display depleted Mn, Ca, and P concentrations (Table 1). Mean EF_{Mn}, EF_{Ca}, and EF_P values in the white limestones (11 samples) are 1.27, 1.15, and 1.12, respectively, but they are 0.65, 0.81, and 0.83 in the red limestones (9 samples) (Fig. 5).

FeO values average 0.13 wt% in the red limestones, similar to values in the white limestones (average 0.12 wt%). Fe_2O_3 in the red limestones ranges from 0.12 wt% to 0.41 wt% with an average of 0.22 wt%, which is significantly higher than in the white limestones, where Fe_2O_3 values range from 0.02 wt% to 0.19 wt% with an average of 0.12 wt%. Total iron in the red limestones ranges from 0.26 to 0.55% with an average of 0.36 wt%, and it ranges from 0.18 wt% to 0.32 wt% in the white limestones with an average of 0.25 wt%. Therefore, the increase in total iron in the red limestones is the result of the increase in Fe_2O_3.

Trace Elements

Several redox-sensitive elements, such as Co, Cr, Cu, Ni, V, and Zn, and detrital-input-sensitive elements (i.e., Rb, Zr) are present in low concentrations in the studied carbonate samples; Ba and Sr concentrations in the analyzed limestones are high (Ba 294.96 μg/g on average and up to 1.3 wt%; Sr 492.34 μg/g on average) (Table 1). Generally, detrital-input-sensitive elements

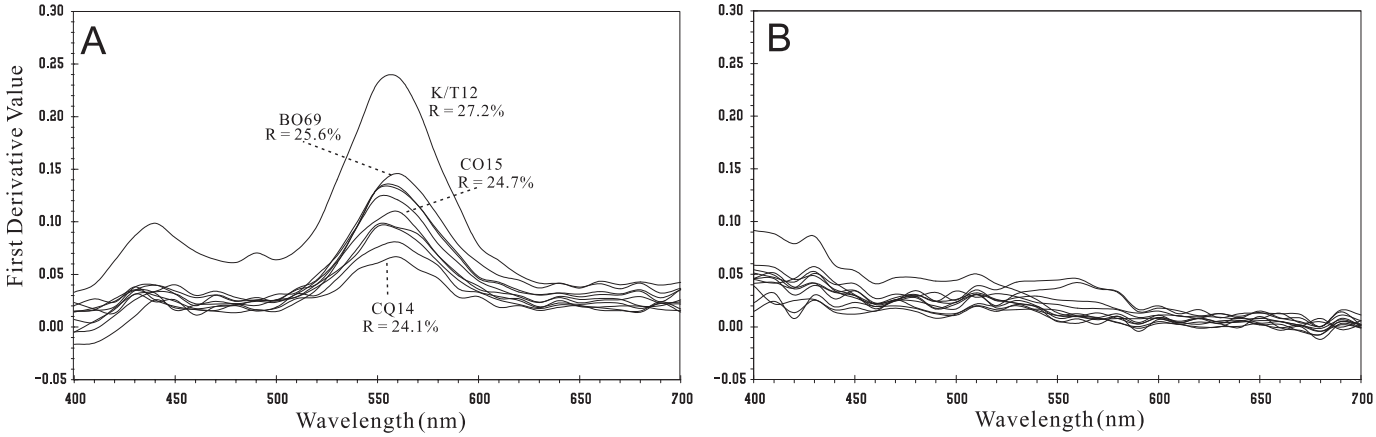

FIG. 3.—First-derivative peaks of diffuse reflectance spectrometry (DRS) for the red and white limestones from the Vispi Quarry section; **A)** Red/pink; **B)** White. Note that in Part A, peak height of hematite at 565 nm increases visibly when the redness increases; R, redness.

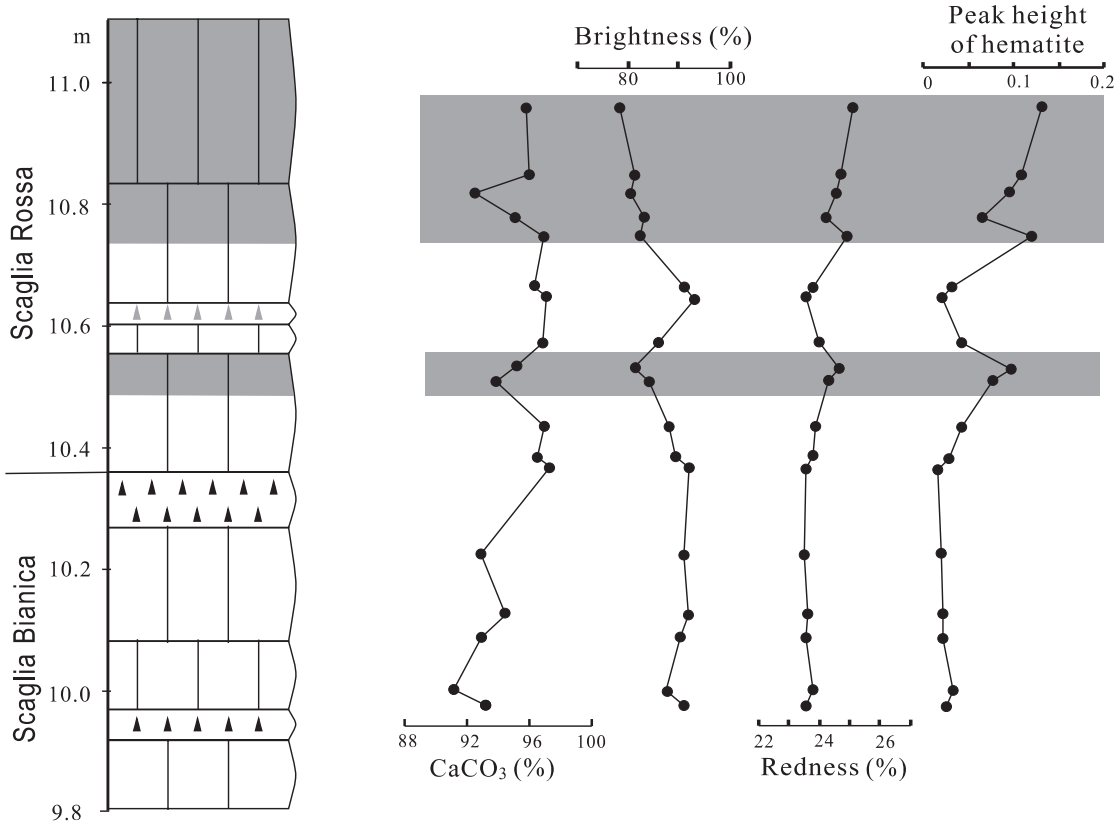

FIG. 4.—Data on carbonate and DRS from the transition interval from the Scaglia Bianica to Scaglia Rossa at the Vispi Quarry section.

show no significant difference between red and white limestones in the Vispi Quarry section. However, the redox-sensitive elements V, Cr, Ni, U and the micronutrients Cu and Zn show minor enrichments in the white limestones. EF_V, EF_{Cr}, EF_{Ni}, EF_{Cu}, EF_U, and EF_{Zn} values are 0.84, 0.71, 0.79, 0.54, 0.97, and 0.69 in red limestones, and are 1.10, 1.19, 1.17, 1.31, 1.14, and 1.02 in white limestones, respectively (Table 1). However, Ba is slightly enriched in red limestones, with $EF_{Ba} = 1.13$, and in white limestones it is 0.91 (Table 1). There is a very high Ba peak (about 1276 μg/g) at 10.85 m (CQ15) above the top of the Bonarelli Level within the red limestones (Appendix 1), due either to analytic error or to a very high content of authigenic barite.

Rare Earth Elements

The ∑REE is relatively low in the analyzed limestones, ranging from 13.06 μg/g to 41.07 μg/g, with an average of 21.04 μg/g (Table 1). Because the marine carbonate phase generally contains significantly less REE than detrital clay and heavy minerals (Piper, 1974), lower ∑REE values in the analyzed limestones suggest strong dilution of the terrigenous component by biogenic calcite. There is no obvious difference in the ∑REE values between red and white limestones.

We normalized the concentration of rare earth elements in our studied carbonates to the REE concentrations of post-Archean Australian sedimentary rocks (PAAS; McLennan, 1989). Overall, the PAAS-normalized REE patterns of studied limestones exhibit seawater-like REE distribution patterns characterized by small enrichments in heavy REE (HREE) relative to light REE (LREE) with negative cerium anomalies (Fig. 6).

The Ce anomaly is calculated according to Wilde et al. (1996): Ce anomaly = $\log [2Ce_n / (La_n + Pr_n)]$, where n is the shale-normalized concentration. Limestone samples from the Vispi Quarry section have an average of δCe = 0.34, ranging from 0.28 to 0.42 (Table 1), very similar to those of typical oceanic seawater (δCe values ranging from < 0.1 to 0.4; Elderfield and Greaves, 1982). The red limestones show REE pattern and δCe values very similar to those of the white limestones (Fig. 6).

DISCUSSION

Nature of Sediments

In the sediments, aluminum can be considered as an indicator of the aluminosilicate fraction, representing detrital input, which is usually immobile during diagenesis (see Calvert and Pedersen, 1993). In the analyzed limestones, Al_2O_3 concentrations are very low, only 0.19–1.14 wt% (Table 1), which indicates that terrigenous detrital input in the Vispi Quarry section was low, perhaps owing to the large distance from the paleo-shoreline, in agreement with the pelagic origin of the limestones (Kuhnt, 1990; Premoli Silva and Sliter, 1994; Montanari and Koeberl, 2000).

Our geochemical results indicate that many of the common conservative lithogenic elements (i.e., Ti, K, Mg, Rb, Zr), when plotted against Al_2O_3, generally have good correlation coefficients (e.g., $R^2 = 0.83$ for K_2O, $R^2 = 0.53$ for MgO, Fig. 7A, B). This points to a homogeneous source area. The Al-normalized Ti and Rb concentrations show almost no obvious change throughout the transition from the Scaglia Bianica to the Scaglia Rossa (Fig. 8).

TABLE 1.—Geochemical parameters of the red limestones and white limestones in the Vispi Quarry section, Italy.

element/oxide	Vispi Quarry Section						Avarage value of the section	
	Red/Pink Limestone			White Limestone				
	concentration	/Al	EF	concentration	/Al	EF	concentration	/Al
$CaCO_3$ (a)	94.69	—	—	94.94	—	—	94.83	—
SiO_2	3.29	5.81	0.84	3.59	7.83	1.13	3.45	6.92
$SiO_{2(excess)}$ (b)	1.41	—	—	2.11	—	—	1.81	—
Al_2O_3	0.59	—	—	0.42	—	—	0.50	—
Fe_2O_3	0.22	0.53	—	0.12	0.39	—	0.16	0.45
FeO	0.13	0.38	—	0.12	0.51	—	0.12	0.45
TFe_2O_3	0.36	0.91	1.01	0.25	0.90	1.00	0.30	0.90
MgO	0.38	0.86	0.83	0.37	1.18	1.13	0.37	1.04
CaO	53.34	147.18	0.81	53.48	210.03	1.16	53.42	181.75
Na_2O	0.03	0.08	0.88	0.03	0.10	1.14	0.03	0.09
K_2O	0.15	0.44	0.93	0.12	0.49	1.04	0.13	0.47
MnO	0.06	0.18	0.65	0.08	0.36	1.27	0.07	0.28
P_2O_5	0.03	0.05	0.83	0.03	0.07	1.12	0.03	0.06
TiO_2	0.02	0.05	0.96	0.02	0.05	1.03	0.02	0.05
V	5.53	19.33	0.84	5.62	25.93	1.10	130.00	22.93
Cr	6.75	24.86	0.71	8.70	42.56	1.19	90.00	35.12
Co	2.15	7.02	1.02	1.24	6.22	0.99	19.00	6.88
Ni	4.07	12.45	0.79	4.53	18.14	1.17	68.00	15.72
Cu	6.24	22.92	0.54	14.43	60.16	1.31	45.00	42.31
Zn	19.92	81.65	0.97	15.08	85.22	1.02	95.00	84.58
Rb	3.81	12.91	1.00	2.88	12.87	1.00	140.00	12.94
Sr	523.47	1941.96	0.88	473.55	2397.74	1.08	300.00	2216.45
Zr	3.60	11.86	1.00	2.60	11.84	1.00	160.00	11.87
Mo	0.76	2.89	0.69	1.05	5.15	1.21	1.30	4.19
Ba	404.21	1824.22	1.13	197.78	1373.01	0.91	580.00	1609.21
U	0.10	0.32	0.79	0.10	0.48	1.14	3.70	0.40

All oxides and bulk parameters are reported as %, minor and trace elements in µg/g.

All trace element/Al are expressed as $*10^{-4}$.

(a) Calculated from the CaO values using an oxide conversion factor of 1.7751.

(b) Calculated assuming (Si/Al)detrital = 3.11 from Wedepohl (1971)

The three most major chemical components, Al_2O_3 (representing clay minerals), SiO_2 (quartz and/or biogenic opal), and CaO (representing calcium carbonate), are plotted in a triangular diagram (Fig. 9). Arbitrary multipliers ($Al_2O_3 * 5$ and CaO/10) are introduced in order to center the data on the graph. Average shale plots close to the SiO_2–$Al_2O_3 * 5$ side in this diagram (Fig. 9). Sediments consisting of a mixture of average shale (AS) and calcium carbonate plot along the connecting line between CaO/10 and the average-shale point. The limestones from the Vispi Quarry section show a distinct distribution pattern along the carbonate-dilution line (from the AS to the CaO pole), indicating that terrigenous clastics represent background sedimentation. In comparison, the red limestones plot closer to the carbonate-dilution line, whereas the white limestones plot closer to the SiO_2 pole, indicating SiO_2 dilution effects (Fig. 9).

Paleoceanographic Redox Changes

Major Elements Fe and Mn.—

Fe in sea water and sediments has two valence states, Fe^{2+} and Fe^{3+}. In strongly anoxic conditions, Fe is divalent and deposited as pyrite (Lyons and Severmann, 2006). In oxic conditions trivalent Fe dominates and forms hematite. The variety of Fe^{3+}/TFe may reflect a variety of redox condition (Haese et al., 1998; Konig et al., 1999; Giosan et al., 2002). Konig et al. (1999, 2001) suggested that Fe^{2+} in clay lattice can be oxidized to Fe^{3+} while in contact with pore water O_2 or NO_3^-. Turgeon and Brumsack (2006) suggested that, compared with Bonarelli Level, Scaglia Bianica white limestones reflect oxic bottom-water conditions. In the Vispi Quarry section, the correlation between TFe and Al_2O_3 ($R^2 = 0.66$, Fig. 7D) indicates that Fe most likely resides in terrigenous clay minerals. The average Fe^{3+}/TFe in red limestones is 0.59, and is generally higher than in white limestones (average $Fe^{3+}/TFe = 0.45$) (Fig. 8). This supports findings from DRS data and indicates that the iron in the red limestones is trivalent and reflects oxic conditions.

Mn can be used as a redox proxy (Calvert and Pedersen, 1993, 1996). Low Mn contents can be indicative of dysoxic bottom-water conditions given that, under reducing conditions at the

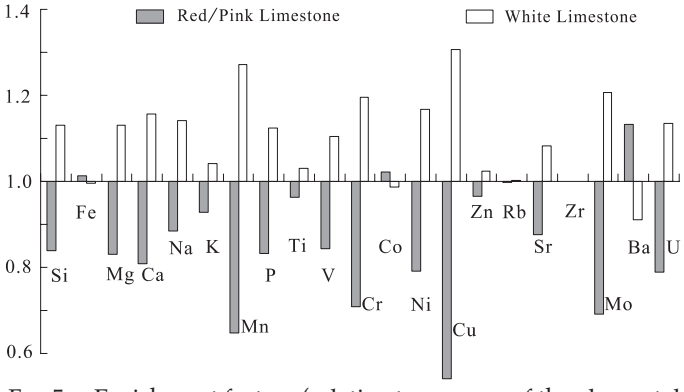

FIG. 5.—Enrichment factors (relative to average of the elemental concentration in the section) of analyzed elements in the Vispi Quarry section.

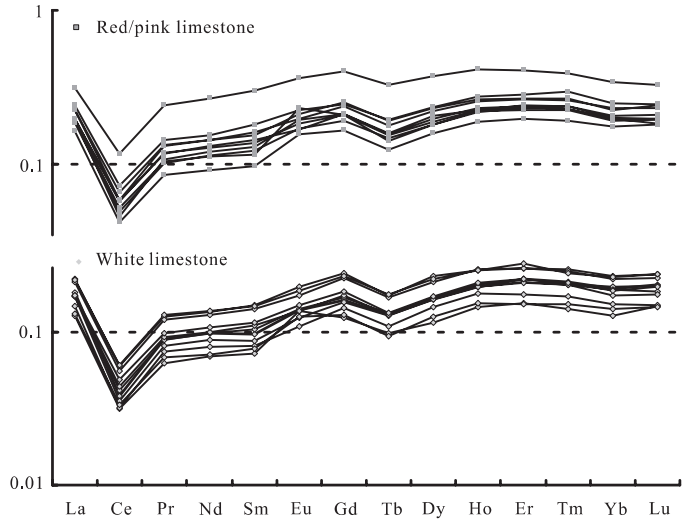

FIG. 6.—The Post-Archean average Australian shale (PAAS)–normalized REE patterns for the limestones in the Vispi Quarry section.

sediment–water interface, soluble Mn^{2+} (as opposed to the much less soluble Mn^{4+}) diffuses from the sediments into oxygen-depleted bottom waters (Landing and Bruland, 1987). In oxic conditions, Mn is deposited as Mn^{4+} oxide/hydroxide, enriched in surface sediments. Calvert and Pedersen (1993, 1996) suggested that the presence of Mn carbonate in marine sediments indicates sedimentation under oxygenated bottom-water conditions. According to Turgeon and Brumsack (2006), Mn is highly enriched in Scaglia Bianica white limestones. In this study, the positive correlation of Mn/Al and Ca/Al (Fig. 7C) shows that Mn resides in the carbonate phase, most likely as Mn carbonate. Mn is depleted in red limestones ($EF_{Mn} = 0.65$) and enriched in white limestones (Fig. 8), which might be caused by more oxic conditions (Calvert and Pedersen, 1993, 1996).

Trace Elements U, V, Cr, Co, Ni, Zn, and Cu.—

U in seawater is present mainly as U^{6+} in the conservative form of uranyl ions that bind to carbonate ions, forming $UO_2(CO_3)_3^{4-}$. In oxic marine settings, dissolved U^{6+} is not reduced to the thermodynamically favored U^{4+}, nor is it scavenged by particulates (Anderson et al., 1989). Reduction of U^{6+} to U^{4+} occurs under conditions of pH and alkalinity similar to Fe^{3+} to Fe^{2+} reduction in seawater (Morford et al., 2001; Chaillou et al., 2002). Because the enrichment takes place within the sediment and not in the water column, the oxygen-penetration depth and the sedimentation rate may play important roles, such that a slower sedimentation rate allows more time for diffusion of uranyl ions from the water column into the sediment (Crusius and Thomson, 2000). In our analyzed samples, U is not obviously enriched in limestones, which may reflect the condition of oxic bottom water. Additionally, $EF_U = 0.79$ in red/pink limestone is depleted relative to AS, compared with white limestone ($EF_U = 1.14$) (Fig. 5), suggesting a more oxic environment of deposition.

V, Cr, Co, and Ni are other redox-sensitive elements. In oxygenated waters, the stable form of V^{5+} is vanadate, $H_2VO_4^{2-}$. Vanadate adsorbs to both Mn and Fe oxyhydroxides (Wehrli and Stumm, 1989). Under slightly reducing conditions, V^{5+} is reduced to V^{4+} and forms vanadyl ions (VO^{2-}), related hydroxyl species $VO(OH)^{3-}$, and insoluble hydroxides $VO(OH)_2$. Under more reducing conditions, H_2S reduces V to V^{3+}, which can be taken up by geoporphyrins or be precipitated as a solid oxide V_2O_3 or hydroxide $V(OH)_3$ phase (Wanty and Goldhaber, 1992). Cr is present mainly as Cr^{6+} in the chromate anion (CrO_4^{2-}) in oxic

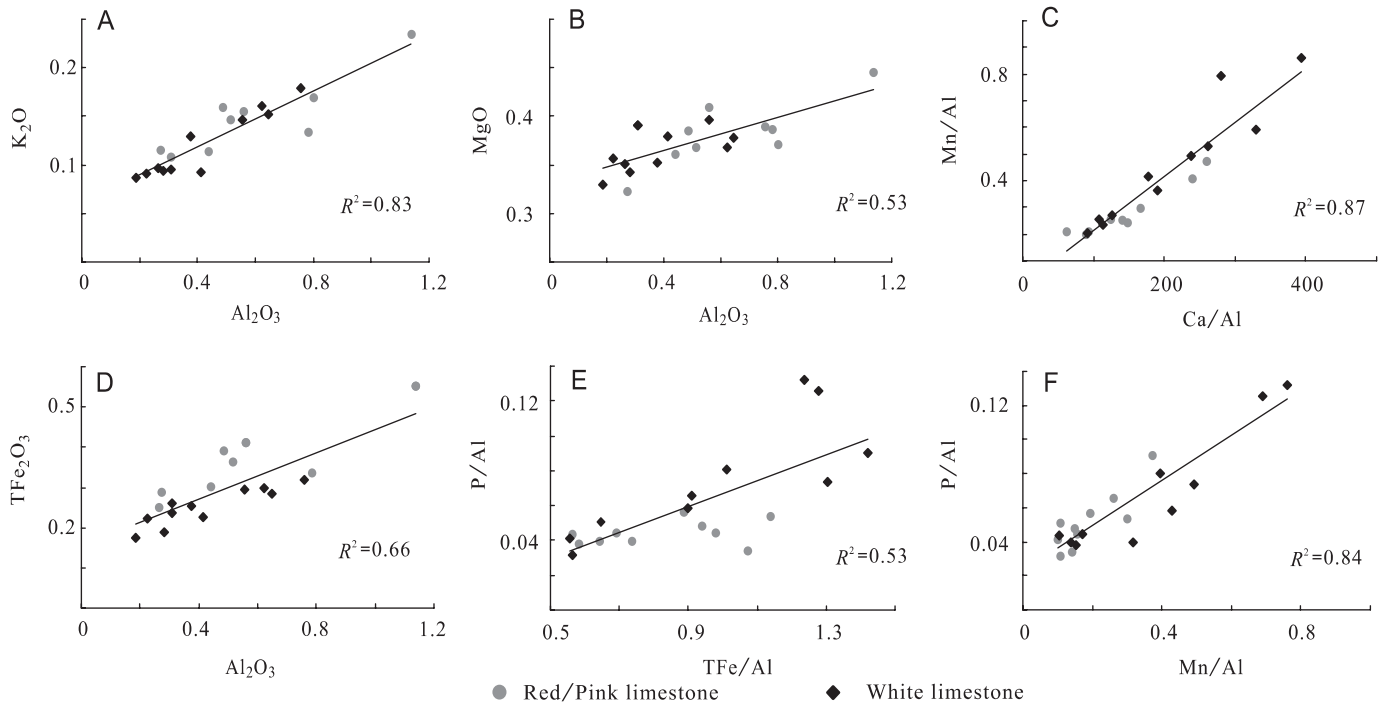

FIG. 7.—Element-relationship diagram for the limestones from the Vispi Quarry section compared to Al_2O_3.

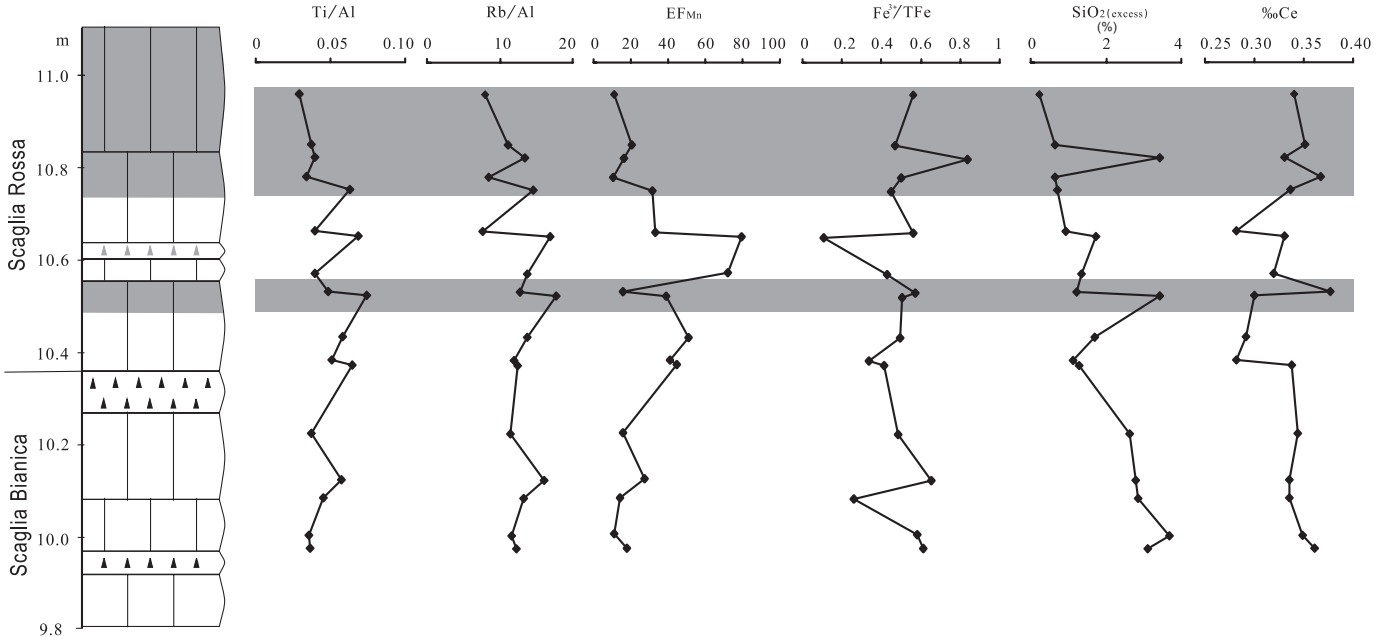

FIG. 8.—Element concentrations and element ratios of selected geochemical proxies in the transition from Scaglia Bianca to Scaglia Rossa at the Vispi Quarry section.

environments (Calvert and Pedersen, 1993). Under normal seawater conditions, chromate anion is soluble, but under anoxic conditions Cr^{4+} is reduced to Cr^{3+}, forming aquahydroxyl cations and hydroxyl cations (e.g., $Cr(OH)^{2+}$), which can be precipitated as insoluble $Cr(OH)_3$, or Cr_2O_3 is adsorbed to Fe and Mn oxyhydroxides (Algeo, 2004). In oxic environments Co is present as the dissolved cation (Achterberg et al., 2003). In anoxic waters, Co forms insoluble CoS, which can be taken up in solid solution by authigenic Fe sulfides (Huerta-Diaz and Morse, 1992). Co behaves similarly to Mn in seawater (Knauer et al., 1982) and in sediments (Hem et al., 1989), hence Co can diffuse out of sediments under reducing conditions (Heggie and Lewis, 1984). In oxic environments, Ni may exist as Ni^{2+} or $NiCl^{+}$ ions (Calvert and Pedersen, 1993). Removal of Ni to the sediment may be accelerated by complexing and sedimentation with organic matter. Remineralization of the organic matter at or below the sediment–water interface may liberate Ni to sediment pore waters.

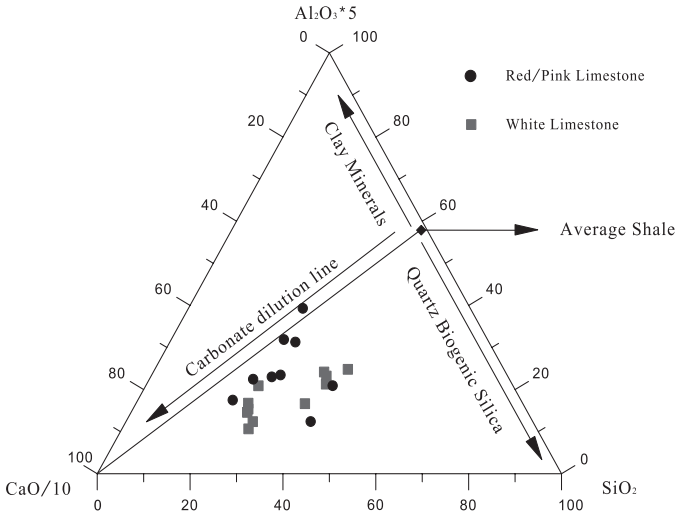

FIG. 9.—Ternary diagram of relative proportions (%) of Al_2O_3 (* 5), SiO_2, and CaO (/10). An arbitrary multiplier of 5 is used for Al_2O_3 to compensate for the low Al concentration, and a division by 10 for CaO, in order to better distribute the data points within the graph. "Average shale" (AS) composition is also shown (Wedepohl, 1971).

In the Vispi Quarry section, the concentrations of V, Ni, Cr, and Co are very low (Table 1). Their enrichment factors show some difference between red/pink limestone and white limestone. V, Ni, Cr, and Co are depleted in the red limestones (EF_V = 0.84, EF_{Ni} = 0.79, EF_{Cr}=0.71) but enriched in white limestone (EF_V = 1.1, EF_{Ni} = 1.17, EF_{Cr}=1.19) indicating oxic-water conditions for the red limestones. EF_{Co} values in red/pink limestones and white limestones are very close, which may indicate a detrital origin of Co.

Further, Zn and Cu are nutrient-related elements. In oxic environments, Zn may exist as Zn^{2+} or $ZnCl^{+}$ (Calvert and Pedersen, 1993), In anoxic waters, dissolved Zn is rapidly precipitated as ZnS in solid solution in pyrite or sometimes as an independent authigenic sphalerite phase (Morse and Luther, 1999). Cu is present mainly in organic–metal ligands and, to a lesser degree, in solution as $CuCl^{+}$ in oxic environments (Calvert and Pedersen, 1993; Achterberg et al., 1997). Release of Cu through remineralization of organic matter by sulfate-reducing bacteria or reductive dissolution of Fe-Mn-oxyhydroxides may liberate Cu within the sediment or at the sediment–water interface. Under anoxic conditions, it may be reduced from Cu^{2+} to Cu^{+} with subsequent precipitation as an independent sulfide phase (CuS or Cu_2S) or uptake by Fe sulfides in solid solution (Achterberg et al., 1997; Morse and Luther, 1999).

The concentration of Cu and Zn is low in all samples. EF_{Cu} and EF_{Zn} values in red limestones are 0.54 and 0.97, which are lower

than in white limestones (1.31 and 1.02), indicating that red limestone was deposited under more oxic conditions.

Trace-element indices Ni/Co and V/Cr have been used to evaluate paleoredox conditions (Jones and Manning, 1994). Ni/Co ratios below 5 suggest oxic conditions, 5–7 dysoxic conditions, and >7 suboxic to anoxic conditions; similarly V/Cr ratios of < 2 suggest oxic conditions, 2–4.25 dysoxic conditions, and > 4.25 suboxic to anoxic conditions. Hatch and Leventhal (1992) suggested that V/(V+Ni) greater than 0.84 indicates euxinic conditions, 0.54–0.82 anoxic waters, and 0.46–0.60 dysoxic conditions. In the Vispi Quarry section, average Ni/Co and V/Cr values are 0.7 and 3.2 in white limestone and 0.8 and 1.8 in red limestones, both indicating oxic deep-water conditions. Averaged V/(V+Ni) ratios are 0.6 in both red and white limestone. On cross-plots of trace-element and Fe^{3+}/TFe ratios, all red limestones plot at values of Ni/Co < 2.5, V/Cr < 1.2, V/(V+Ni) < 0.6, and Fe^{3+}/TFe > 0.45 (Fig. 10), while white limestones are more dispersed. This again suggests that the red limestones were deposited in more oxygenated waters than white limestones.

Ce Anomaly.—

Unlike the other REE, cerium can undergo oxidation in seawater from soluble Ce^{3+} to the highly insoluble quadrivalent state. Its subsequent fixation in particulate matter, including organics, is thought to be responsible for distinctive depletion of Ce in well-oxygenated seawater. The Ce anomaly has been adopted as a sensitive tracer for paleoceanographic redox conditions (see Pattan et al., 2005).

Rare earth elements (REE) of the pink/red and white limestones in the Vispi Quarry section have very similar shale-normalized patterns with HREE enrichments and negative Ce anomalies. Limestone samples from the Vispi Quarry section have an average of δCe = 0.34, ranging from 0.28 to 0.42, which is very similar to typical oceanic seawater values (δCe values ranging from < 0.1 to 0.4; Elderfield and Greaves, 1982). This indicates that limestones of the Vispi Quarry section have a clear dependence on the REE chemistry of the seawaters, and were deposited under oxic bottom-water conditions.

The red limestones show REE patterns and δCe values very similar to those of the white limestones (Fig. 8). This implies that redox change at the sediment–water interface, which resulted in the red color of the limestones, affected neither REEs nor their patterns. In other words, the δCe proxy is not sensitive enough to record the inferred redox change recorded by the color change from white to red.

Primary Productivity.—

$SiO_{2(excess)}$, P, and Ba have often been used as paleoproductivity proxies (Schmitz et al., 1997). In marine sediments, the sources of SiO_2 are terrigenous Al silicates, quartz, and opal (biogenic silica) (Treppke et al., 1996). $SiO_{2(excess)}$ concentration represents a rough estimate of opaline silica content and can be calculated using

$$SiO_{2(excess)} = SiO_{2(sample)} - [(SiO_2 / Al_2O_{3(background)} \times Al_2O_{3(sample)}]$$

Schmitz et al. (1997) showed a positive correlation between $SiO_{2(excess)}$ and $\delta^{13}C$, Ba, and P; therefore $SiO_{2(excess)}$ can be used as a paleoproductivity proxy. P is a nutrient, and its content in sediments is used as an indicator of paleoproductivity controlled by the availability of active P (Tyrrell, 1999). Recent marine studies indicate that in high-productivity areas (e.g., regions of upwelling), sediments are commonly enriched in P (Föllmi, 1996; Brumsack, 2006). Similarly, Ba has been proposed as a proxy for productivity (Dymond et al., 1992). However, sedimentary barite might undergo diagenetic changes and should be used cautiously as a proxy (McManus et al., 1998).

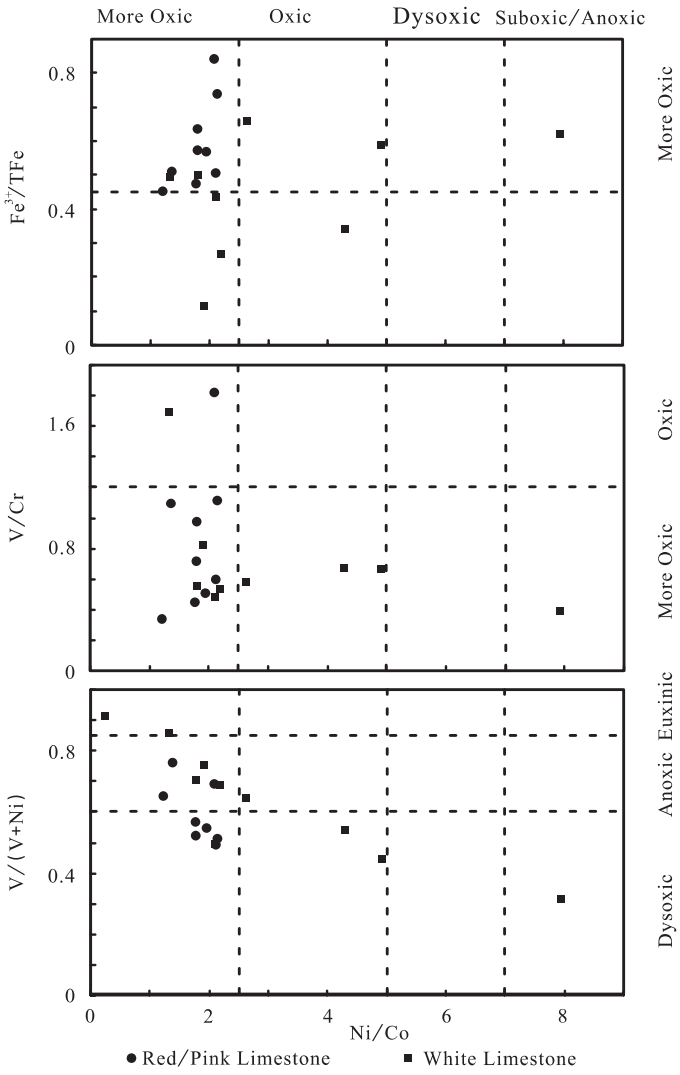

FIG. 10.—Plots of Ni/Co vs. Fe^{3+}/TFe, Ni/Co vs. V/Cr, and Ni/Co vs. V/(V+Ni). Red limestones plot at values of Ni/Co < 2.5, V/Cr < 1.2, V/(V+Ni) < 0.6, and Fe^{3+}/TFe > 0.45, whereas white limestones are more dispersed, suggesting that the red limestones were deposited in more oxygenated waters than were white limestones.

In the Vispi Quarry section, all limestones samples have positive $SiO_{2(excess)}$, but their concentrations are very low (Fig. 8). P concentrations are low in the limestones but Ba concentrations are high. Enrichment factors show that $EF_P = 0.83$ and $EF_{Ba} = 1.13$ in red limestones, and are close to those in white limestones ($EF_P = 1.12$ and $EF_{Ba} = 0.91$). Turgeon and Brumsack (2006) suggested that Scaglia Bianica white limestones perhaps reflect high productivity. However, in this study the productivity proxies show no significant differences between red and white limestones. Because P/Al vs. TFe/Al and P/Al vs. Mn/Al correlate well (Fig. 7E, F) in all limestones, the enrichment of P may be related to the Fe and Mn cycles.

Origin of Red Color

The color of pelagic sediments is an indication of redox conditions on the sea floor (Wilson et al., 1985; Thomson et al., 1987; Giosan et al., 2002). The red color is a postdepositional feature and requires prolonged exposure of sediments to oxygen-rich bottom water (Thomson et al., 1987; Krenmayr, 1996; Jansa and Hu, this volume). Field observations in the Vispi Quarry section show that the reddish Scaglia Rossa strata are bedded and in undisturbed contact with the underlying whitish-colored strata. Within a single red bed the color is uniform, which indicates that the color resulted from synsedimentary or early diagenetic processes. Color variations from white to red usually coincide with bedding planes, but locally they occur within single beds, such as the two transitional beds (Fig. 2), in which from bottom to top the color changes from white to pink and red (Hu et al., 2006a). The distribution of red coloration strongly indicates that color is the product neither of weathering nor of detrital origin, because the detrital-sensitive Al elements and Al-normalized proxies (Ti/Al and/or Rb/Al) in the white beds are the same as those in red beds (Fig. 8). This also indicates a common homogeneous source area for white and red limestones. Our conclusion is supported by Eren and Kadir (1999), who investigated the Upper Cretaceous pelagic red sediments in Turkey. Their electron microscope study showed that the hematite platelets are hexagonal in shape and grew epitaxially on the grains, strongly suggesting their early diagenetic origin.

A comparison of the first-derivative curves of samples with different redness values illustrates that hematite is the source of the red color in the Scaglia Rossa limestones (Fig. 3A). The question remains: how much hematite causes the red color of the CORBs? We have employed two indirect methods to infer the hematite concentration: (1) Fe_2O_3 values average 0.12 wt% in the white limestones, and most probably are a form of iron oxide, such as magnetite. Fe_2O_3 in the red limestones averages 0.22 wt% and may be present as both magnetite and hematite. Assuming that magnetite content in both red and white limestones may be the same because they had a homogeneous source area and terrigenous input, we suggest that a 0.1% difference of Fe_2O_3 content between red and white limestones can be attributed to hematite. (2) Deaton and Balsam (1991) determined hematite concentrations by DRS of calcite, quartz, simulated North Atlantic matrix, and simulated Gulf of Mexico matrix by analyzing a series of standards that contain concentrations of hematite ranging from 0.01% to 1%. Because the limestones in the Scaglia Rossa are composed mainly of calcite (about 95% $CaCO_3$ on average) with minor clay minerals (mainly illite–smectite mixed-layer, illite, trace kaolinite, and chlorite) (Johnsson and Reynolds, 1986), we suggest that the Scaglia Rossa limestones have a matrix between purely calcite and the simulated North Atlantic matrix. Hematite concentrations of 0.05% and 0.1% for simulated North Atlantic matrix have a peak height of hematite about 0.1 and 0.18 at the first-derivative curve, respectively, and hematite concentrations of 0.01% and 0.05% for calcite have a peak height of hematite about 0.15 and 0.4, respectively (Deaton and Balsam, 1991). Because the peak heights of hematite in pink/red limestones in the Vispi Quarry section are about 0.05–0.15 with an average of 0.12, we suppose that ~ 0.1 wt% hematite is responsible for the red/pink limestones in the Vispi Quarry section.

Channell et al. (1982) studied magnetic properties of the Upper Cretaceous Scaglia Rossa red pelagic limestones in the Bottaccione Gorge section, Italy, and found that the boundaries of paleomagnetic reversals defined by hematite are a few tens of centimeters below those of magnetite. Therefore, they interpreted that hematite grains were magnetized in the post-reversal field, which demonstrates that growth of hematite crystals occurred over ~ 10^5 years during early diagenesis.

Sedimentary Models for CORBs

Based on our mineralogical and inorganic geochemical data, we propose a depositional model for Vispi Quarry red and white limestones (Fig. 11). The redox state at the sediment–water interface is controlled by the rate of organic-carbon deposition and respiration, which controls the concentration of dissolved oxygen in the sediment pore waters. The redox state is further controlled by oxygen concentration in the bottom water itself. Changes in either of these properties result in a change of the redox state at the sediment–water interface (Kaiho, 1994; Morford and Emerson, 1999). As discussed above, conditions at the sediment–water interface were more oxic during deposition of red limestone than of white limestone. $SiO_{2(excess)}$ and proxies for P and Ba productivity show that there are no significant differences in paleoproductivity between red limestone and white limestone. Thus an increase in dissolved oxygen in bottom waters would be the most probable cause of the origin of the red coloration. Considering that the detrital input and source area of the red limestones are the same for both of the limestones, we suggest that intensified bottom circulation may have been responsible for more oxic conditions at the sea floor , as suggested by Hu et al. (2005), Hu et al. (2006a), and Hu et al. (2006b). The mid-Cretaceous was a period of rapid sea-level fluctuations and tectonic disturbance (e.g., Ricou, 1996), resulting in dramatic paleogeographic changes. Tectonic changes and changes in the ocean-basin topography could have contributed to changes in bottom-water circulation patterns and result in the inflow of colder, more oxygenated deep waters to some of the western Tethys subbasins (Poulsen et al., 1998; Hu et al., 2006a).

CONCLUSIONS

(1) The limestones from the Vispi Quarry section represent simple background shale sedimentation diluted by carbonates. Very low Al_2O_3 concentrations (0.19–1.14 wt%) indicate that terrigenous detrital input in the Vispi Quarry section was relatively low. Many of the common conservative lithogenic elements (i.e., Ti, K, Mg, Rb, Zr) lie close to AS when plotted against Al_2O_3, pointing to a homogeneous source area. Terrigenous detrital input and source area did not change throughout the transition from the Scaglia Bianica to the Scaglia Rossa.

(2) Geochemical data show that, for red limestones, conditions at the sediment–water interface were more oxic than for the white limestones in the Vispi Quarry section. This conclusion is supported by: (1) high Fe_2O_3 values (0.22% on average) and high Fe^{3+}/TFe ratio (0.58); (2) low EF values of redox-sensitive elements U, V, Cr, Co, and Ni in the red limestones, with ratios of $Ni/Co < 2.5$, $V/Cr < 1.2$, $V/(V+Ni) < 0.6$, and $Fe^{3+}/TFe > 0.45$; and (3) a strongly negative δCe anomaly (0.28–0.42).

(3) The red color of the limestones is the product neither of weathering nor of detrital input. The positive correlation between the peak height of hematite and redness values indicates that hematite concentration is a cause not only of the hue of the red color but also of the deepness of the red color in the Vispi Quarry limestones. The DRS data indicate that the red color of the Scaglia Rossa limestones is a result of a low concentration (~ 0.1 wt %) of finely dispersed hematite.

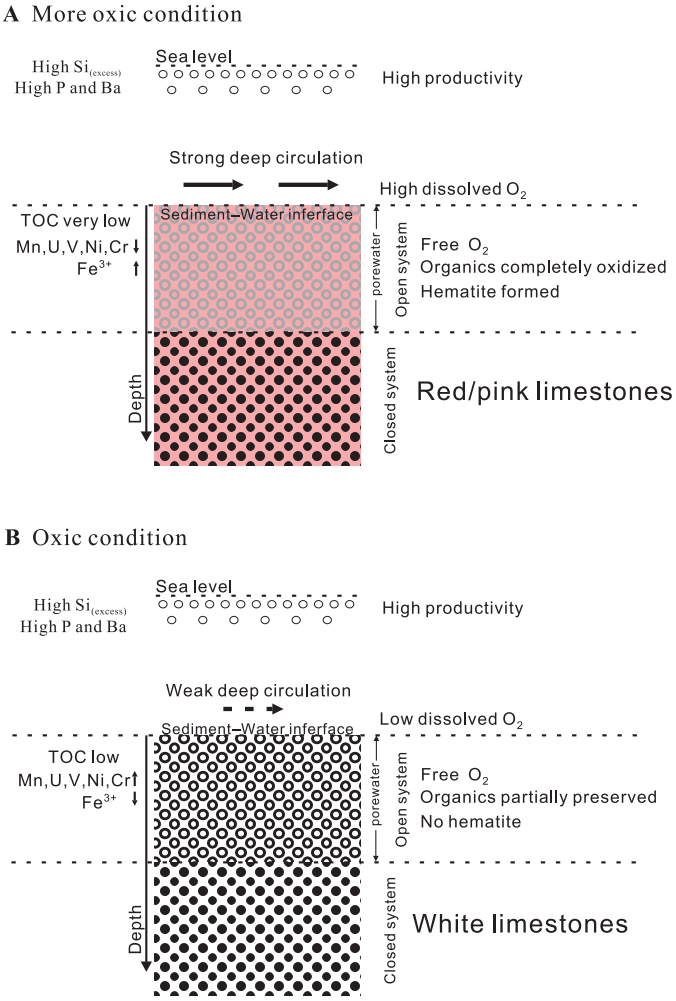

FIG. 11.—Depositional model for the limestones in the Vispi Quarry section. A) Red limestones deposited in more oxic condition. Organic matter is completely oxidized in pore water below the sediment–water interface. In the red limestones, TOC is very low, contents of elements Mn, U, V, Ni, and Cr decrease, while Fe^{3+} content increases and hematite forms. Most probably, intensified bottom circulation was responsible for more oxic conditions which resulted in more dissolved free O_2 at the sea floor. B) White limestones deposited in oxic condition. Organic matter is partially preserved, and no hematite forms. In white limestones, TOC is low, contents of elements Mn, U, V, Ni, and Cr increase, while Fe^{3+} contents decrease.

(4) $SiO_{2(excess)}$, P, and Ba productivity proxies show that there were no significant differences in paleoproductivity between deposition of red and white limestone. An increase in dissolved oxygen in bottom waters was most probably the main cause for the origin of the red limestones. We suggest that intensified bottom circulation may have resulted in more oxic bottom conditions.

ACKNOWLEDGMENTS

We are thankful to Profs. Chengshan Wang and Xuexiang Gu for general support. We are grateful to Mr. Zhang Mengqun (XRF), and Mr. Gao Jianfeng (ICP-MS) from Nanjing University, who aided our geochemical and mineralogical laboratory work. We are thankful to Prof. Luba Jansa and Prof. Robert Scott for their helpful comments and English revision. We are deeply grateful to Michael Wagreich and Stephanie Neuhuber for their constructive, valuable comments. I (X. Hu) would like to present this paper as a special gift to my newborn daughter—Heran. This study was financially supported by the Ministry of Science and Technology, China 973 Project (2006CB701402) and the National Natural Science Foundation, China Project (40332020 and 40625012). This is a contribution to the International Geosciences Project 494.

REFERENCES

ACHTERBERG, E.P., VAN DEN BERG, C.M.G., BOUSSEMART, M., AND DAVISON, W., 1997, Speciation and cycling of trace metals in Esthwaite water: a productive English lake with seasonal deep-water anoxia: Geochimica et Cosmochimica Acta, v. 61, p. 5233–5253.

ACHTERBERG, E.P., VAN DEN BERG, C.M.G., AND COLOMBO, C., 2003, High resolution monitoring of dissolved Cu and Co in coastal surface waters of the western North Sea: Continental Shelf Research, v. 23, p. 611–623.

ALGEO, T.J., 2004, Can marine anoxic events draw down the trace element inventory of seawater?: Geology, v. 32, p. 1057–1060.

ANDERSON, R.F., FLEISHER, M.Q., AND LEHURAY, A.P., 1989, Concentration, oxidation state and particulate flux of uranium in the Black Sea: Geochimica et Cosmochimica Acta, v. 53, p. 2215–2224.

BALSAM, W.L., AND DEATON, B.C., 1991, Sediment dispersal in the Atlantic Ocean: evaluation by visible light spectra: Reviews in Aquatic Sciences, v. 4, p. 411–447.

BALSAM, W.L., AND DEATON, B.C., 1996, Determining the composition of late Quaternary marine sediments from NUV, VIS, and NIR diffuse reflectance spectra: Marine Geology, v. 134, p. 31–55.

BALSAM, W.L., DEATON, B.C., AND DAMUTH, J.E., 1999, Evaluating optical lightness as a proxy for carbonate content in marine sediment cores: Marine Geology, v. 161, p. 141–153.

BRUMSACK, H.J., 2006, The trace metal content of recent organic carbon–rich sediments: Implications for Cretaceous black shale formation: Palaeogeography, Palaeoclimatology, Palaeoecology, v. 232, p. 344–361.

CALVERT, S.E., AND PEDERSEN, T.F., 1993, Geochemistry of recent oxic and anoxic sediments: implications for the geological record: Marine Geology, v. 113, p. 67–88.

CALVERT, S.E., AND PEDERSEN, T.F., 1996, Sedimentary geochemistry of manganese: implications for the environment of formation of manganiferous black shales: Economic Geology, v. 91, p. 36–47.

CHAILLOU, G., ANSCHUTZ, P., LAVAUX, G., SCHÄFER, J., AND BLANC, G., 2002, The distribution of Mo, U, and Cd in relation to major redox species in muddy sediments of the Bay of Biscay: Marine Chemistry, v. 80, p. 41–59.

CHANNELL, J.E.T., FREEMAN, R., HELLER, F., AND LOWRIE, W., 1982, Timing of diagenetic haematite growth in red pelagic limestones from Gubbio (Italy): Earth and Planetary Science Letters, v. 58 p. 189–201.

CRUSIUS, J., AND THOMSON, J., 2000, Comparative behavior of authigenic Re, Mo and U during reoxidation and subsequent long-term burial in marine sediments: Geochimica et Cosmochimica Acta, v. 64, p. 2233–2243.

DEATON, B.C., AND BALSAM, W.L., 1991, Visible spectroscopy: a rapid method for determining hematite and goethite concentration in geological materials: Journal of Sedimentary Petrology, v. 61, p. 628–632.

DYMOND, J., SUESS, E., AND LYLE, M., 1992, Barium in deep-sea sediment: A geochemical proxy for paleoproductivity: Paleoceanography, v. 7, p. 163–181.

ELDERFIELD, H., AND GREAVES, M.J., 1982, The rare earth elements in seawater: Nature, v. 296, p. 214–219.

EREN, M., AND KADIR, S., 1999, Colour origin of Upper Cretaceous pelagic red sediments within the Eastern Pontides, northeast Turkey: International Journal of Earth Sciences, v. 88, p. 593–595.

FÖLLMI, K.B., 1996, The phosphorus cycle, phosphogenesis and marine phosphate-rich deposits: Earth-Science Reviews, v. 40 p. 55–124.

GIOSAN, L., FLOOD, R.D., AND ALLER, R.C., 2002, Paleoceanographic significance of sediment color on western North Atlantic drifts: I. Origin of color: Marine Geology, v. 189, p. 25–41.

HAESE, R.R., PETERMANN, H., DITTERT, L., AND SCHULZ, H.D., 1998, The early diagenesis of iron in pelagic sediments: a multidisciplinary approach: Earth and Planetary Science Letters, v. 157, p. 233–248.

HATCH, J.R., AND LEVENTHAL, J.S., 1992, Relationship between inferred redox potential of the depositional environment and geochemistry of the Upper Pennsyvanian (Missourian) Stark Shale Member of the Dennis Limestone, Wabaunsee County, Kansas, U.S.A.: Chemical Geology, v. 99, p. 65–82.

HEGGIE, D., AND LEWIS, T., 1984, Cobalt in pore waters of marine sediments: Nature, v. 311, p. 453–455.

HEM, J.D., LIND, C.J., AND ROBERSON, C.E., 1989, Coprecipitation and redox reactions of manganese oxide with copper and nickel: Geochimica et Cosmochimica Acta, v. 53, p. 2811–2822.

HU, X.M., JANSA, L., WANG, C.S., SARTI, M., BAK, K., WAGREICH, M., MICHALIK, J., AND SOTAK, J., 2005, Upper Cretaceous oceanic red beds (CORBs) in the Tethys: occurrences, lithofacies, age, and environments: Cretaceous Research, v. 26, p. 3–20.

HU, X.M., JANSA, L., AND SARTI, M., 2006a, Mid-Cretaceous oceanic red beds in the Umbria–Marche Basin, central Italy: Constraints on paleoceanography and paleoclimate: Palaeogeography, Palaeoclimatology, Palaeoecology, v. 233, p. 163–186.

HU, X.M., WANG, C.S., LI, X.H., AND JANSA, L., 2006b, Upper Cretaceous oceanic red beds in southern Tibet: Lithofacies, environments and colour origin: Science in China, Series D, Earth Sciences, v. 49, p. 785–795.

HUERTA-DIAZ, M.A., AND MORSE, J.W., 1992, Pyritisation of trace metals in anoxic marine sediments: Geochimica et Cosmochimica Acta, v. 56, p. 2681–2702.

JI, J.F., BALSAM, W., AND CHEN, J., 2001, Mineralogic and climatic interpretations of the Luochuan loess section (China) based on diffuse reflectance spectrophotometry: Quaternary Research, v. 56, p. 23–30.

JI, J.F., BALSAM, W., CHEN, J., AND LIU, L.W., 2002, Rapid and quantitative measurement of hematite and goethite in the Chinese loess–paleosol sequence by diffuse reflectance spectroscopy: Clays and Clay Minerals, v. 50, p. 208–216.

JOHNSSON, M.J., AND REYNOLDS, R.C., 1986, Clay mineralogy of shale–limestone rhythmites in the Scaglia Rossa (Turonian–Eocene), Italian Appennines: Journal of Sedimentary Petrology, v. 56, p. 501–509.

JONES, B.J., AND MANNING, A.C., 1994, Comparison of geochemical indices used for the interpretation of palaeoredox conditions in ancient mudstones: Chemical Geology, v. 111, p. 111–129.

JUDD, D.B., AND WYSZECKI, G., 1975, Color in Business, Science, and Industry: New York, John Wiley & Sons, 553 p.

KAIHO, K., 1994, Benthic foraminiferal dissolved-oxygen index and dissolved-oxygen levels in the modern ocean: Geology, v. 22, p. 719–722.

KNAUER, G.A., MARTIN, J.H., AND GORDON, R.M., 1982, Cobalt in north-east Pacific waters: Nature, v. 297, p. 49–51.

KONIG, I., HAECKEL, M., DRODT, M., SUESS, E., AND TRAUTWEIN, A.X., 1999, Reactive Fe(II) layers in deep-sea sediments: Geochimica et Cosmochimica Acta, v. 63, p. 1517–1526.

KONIG, I., HAECKEL, M., DRODT, M., SUESS, E., AND TRAUTWEIN, A.X., 2001, A geochemical model of the Peru Basin deep-sea floor and the response of the system to technical impacts: Deep-Sea Research II, v. 48, p. 3737–3756.

KRENMAYR, H.G., 1996, Hemipelagic and turbiditic mudstone facies associations in the Upper Cretaceous Gosau Group of the Northern Calcareous Alps (Austria): Sedimentary Geology, v. 101, p. 149–172.

KUHNT, W., 1990, Agglutinated foraminifera of western Mediterranean Upper Cretaceous pelagic limestones, Umbrian Apennines, Italy, and Betic Cordillera, southern Spain: Micropaleontology, v. 36, p. 297–330.

KUHNT, W., AND HOLBOURN, A., 2005, Late Cretaceous deep-water benthic foraminiferal biofacies and lithofacies of the western and eastern Tethys: Earth Science Frontiers, v. 12(2), p. 81–103.

LANDING, W.M., AND BRULAND, K.W., 1987, The contrasting biogeochemistry of iron and manganese in the Pacific Ocean: Geochimica et Cosmochimica Acta, v. 51, p. 29–43.

LYONS, T.W., AND SEVERMANN, S., 2006, A critical look at iron paleoredox proxies: New insights from modern euxinic marine basins: Geochimica et Cosmochimica Acta, v. 70, p. 5698–5722.

MCLENNAN, S.M., 1989, Rare earth elements in sedimentary rocks: influence of provenance and sedimentary processes, *in* Lipin, B.R., and McKay, G.A., eds., Geochemistry and Mineralogy of Rare Earth Elements: Reviews in Mineralogy, v. 21, p. 169–200.

MCMANUS, J., BERELSON, W.M., KLINKHAMMER, G.P., JOHNSON, K.S., COALE, K.H., ANDERSON, R.F., KUMAR, N., BURDIGE, D.J., HAMMOND, D.E., BRUMSACK, H.J., MCCORKLE, D.S., AND RUSHDI, A., 1998, Geochemistry of barium in marine sediments: implications for its use as a paleoproxy: Geochimica et Cosmochimica Acta, v. 62, p. 3453–3473.

MELINTE, M.C., AND JIPA, D., 2005, Campanian–Maastrichtian marine red beds in Romania: biostratigraphic and genetic significance: Cretaceous Research, v. 26, p. 49–56.

MONTANARI, A., AND KOEBERL, C., 2000, Impact Stratigraphy: The Italian Record: Berlin, Springer, 364 p.

MORFORD, J.L., AND EMERSON, S., 1999, The geochemistry of redox sensitive trace metals in sediments: Geochimica et Cosmochimica Acta, v. 63, p. 1735–1750.

MORFORD, J.L., RUSSELL, A.D., AND EMERSON, S., 2001, Trace metal evidence for changes in the redox environment associated with the transition from terrigenous clay to diatomaceous sediments, Saanich Inlet, BC: Marine Geology, v. 174, p. 355–369.

MORSE, J.W., AND LUTHER, G.W., 1999, Chemical influences on trace metal–sulfide interactions in anoxic sediments: Geochimica et Cosmochimica Acta, v. 63, p. 3373–3378.

PATTAN, J.N., PEARCE, N.J.G., AND MISLANKAR, P.G., 2005, Constraints in using Cerium-anomaly of bulk sediments as an indicator of paleo bottom water redox environment: A case study from the Central Indian Ocean Basin: Chemical Geology, v. 211, p. 260–278.

PIPER, D.Z., 1974, Rare earth elements in the sedimentary cycle, a summary: Chemical Geology, v. 14, p. 285–304.

POULSEN, C.J., SEIDOV, D., BARRON, E.J., AND PETERSON, W.H., 1998, The impact of paleogeographic evolution on the surface oceanic circulation and the marine environment in the mid-Cretaceous Tethys: Paleoceanography, v. 13, p. 546–559.

PREMOLI SILVA, I., AND SLITER, W.V., 1994, Cretaceous planktonic foraminiferal biostratigraphy and evolutionary trends from the Bottaccione section, Gubbio, Italy: Paleontographia Italica, v. 82, p. 1–89.

RICOU, L.E., 1996, The plate tectonic history of the past Tethys Ocean, *in* Nairn, A.E.M., Ricou, L.E., Vrielynck, B., and Dercourt, J., eds., The Ocean Basins and Margins, Volume 8, The Tethys Ocean: New York, Plenum Press, p. 3–70.

SCHLANGER, S.O., AND JENKYNS, H.C., 1976, Cretaceous oceanic anoxic events: cause and consequence: Geolologie en Mijnbouw, v. 55, p. 179–184.

SCHMITZ, B., CHARISI, S.D., THOMPSON, E.I., AND SPEIJER, R.P., 1997, Barium, $SiO_{2\ (excess)}$, and P_2O_5 as proxies of biological productivity in the Middle East during the Palaeocene and the latest Palaeocene benthic extinction event: Terra Nova, v. 9, p. 95–99.

THOMSON, J., COLLEY, S., HIGGS, N.C., HYDES, D.J., WILSON, T.R.S., AND SORENSEN, J., 1987, Geochemical oxidation trends in NE Atlantic

distal turbidites and their effects in the sedimentary record, *in* Weaver, P.P.E., and Thomson, J., eds., Geology and Geochemistry of Abyssal Plains: Geological Society of London, Special Publication 31, p. 167–177.

Torrent, J., and Schwertmann, U., 1987, Influence of hematite on the color of red beds: Journal of Sedimentary Petrology, v. 57, p. 682–686.

Tremolada, F., 2002, Aptian to Campanian calcareous nannofossil biostratigraphy from the Bottaccione section, Gubbio, Central Italy: Rivista Italiana di Paleontologia e Stratigrafia, v. 108, p. 441–455.

Treppke, U.F., Lange, C.B., and Wefer, G., 1996, Vertical fluxes of diatoms and silicoflagellates in the eastern equatorial Atlantic, and their contribution to the sedimentary record: Marine Micropaleontology, v. 28, p. 73–96.

Turgeon, S., and Brumsack, H.J., 2006, Anoxic vs. dysoxic events reflected in sediment geochemistry during the Cenomanian–Turonian Boundary Event (Cretaceous) in the Umbria–Marche Basin of central Italy: Chemical Geology, v. 234, p. 321–339.

Tyrrell, T., 1999, The relative influence of nitrogen and phosphorus on oceanic primary production: Nature, v. 400, p. 525–529.

Van der Weijden, C.H., 2002, Pitfalls of normalization of marine geochemical data using a common divisor: Marine Geology, v. 184, p. 167–187.

Wagreich, M., and Krenmayr, H.G., 2005, Upper Cretaceous oceanic red beds (CORB) in the Northern Calcareous Alps (Nierental Formation, Austria): slope topography and clastic input as primary controlling factors: Cretaceous Research, v. 26, p. 57–64.

Wang, C.S., and Hu, X.M., 2005, Cretaceous world and oceanic red beds: Earth Science Frontiers, v. 12(2), p. 11–21.

Wang, C.S., Hu, X.M., Sarti, M., Scott, R.W., and Li, X.H., 2005, Upper Cretaceous oceanic red beds in southern Tibet: a major change from anoxic to oxic, deep-sea environments: Cretaceous Research, v. 26, p. 21–32.

Wanty, R.B., and Goldhaber, M.B., 1992, Thermodynamics and kinetics of reactions involving vanadium in natural systems: accumulation of vanadium in sedimentary rocks: Geochimica et Cosmochimica Acta, v. 56, p. 1471–1483.

Wedepohl, K.H., 1971, Environmental influences on the chemical composition of shales and clays, *in* Ahrens, L.H., Press, F., Runcorn, S.K., and Urey, H.C., eds., Physics and Chemistry of the Earth: Oxford, U.K., Pergamon, p. 305–333.

Wehrli, B., and Stumm, W., 1989, Vanadyl in natural waters: adsorption and hydrolysis promote oxygenation: Geochimica et Cosmochimica Acta, v. 53, p. 69–77.

Wilde, P., Quinby-Hunt, M.S., and Erdtmann, B.D., 1996, The whole-rock cerium anomaly: a potential indicator of eustatic sea-level changes in shales of the anoxic facies: Sedimentary Geology, v. 101, p. 43–53.

Wilson, A.D., 1960, The micro-determination of ferrous iron in silicate minerals by a volumetric and a colorimetric method: Analyst, v. 85, p. 823–827.

Wilson, T.R.S., Thomson, J., Colley, S., Hydes, D.J., Higgs, N.C., and Sorensen. J., 1985, Early organic diagenesis; the significance of progressive subsurface oxidation fronts in pelagic sediments: Geochimica et Cosmochimica Acta, v. 49, p. 811–822.

APPENDIX 1.—Major-element, trace-element and rare-earth-element concentrations of the limestones in the Vispi Quarry section.

Sample	Lithology	Position	Al_2O_3	CaO	Fe_2O_3	FeO	K_2O	MgO	MnO	Na_2O	P_2O_5	SiO_2	TiO_2	LOI	∑	$CaCO_3$	SiO_2(excess)	TFe_2O_3
K/T12	Dark red limestone	14.80	1.14	52.19	0.41	0.13	0.23	0.44	0.08	0.03	0.07	3.56	0.04	41.06	99.39	92.64	-0.45	0.55
CO-49	Dark red limestone	13.75	0.49	53.76	0.25	0.13	0.16	0.39	0.05	0.03	0.02	2.76	0.02	41.72	99.76	95.44	1.04	0.39
CQ16	Pink limestone	10.96	0.78	53.88	0.19	0.13	0.13	0.39	0.06	0.03	0.03	2.98	0.02	41.78	100.40	95.65	0.22	0.34
CQ15	Pink limestone	10.85	0.44	54.01	0.14	0.14	0.11	0.36	0.06	0.02	0.03	2.19	0.01	42.05	99.57	95.87	0.64	0.30
0924-2-2	Pink limestone	10.82	0.56	52.05	0.35	0.06	0.15	0.41	0.06	0.03	0.03	5.39	0.02	40.51	99.63	92.40	3.41	0.41
CQ14	Light Pink limestone	10.78	0.80	53.40	0.17	0.15	0.17	0.37	0.05	0.03	0.04	3.46	0.02	41.73	100.40	94.79	0.63	0.34
CO-37	Pink limestone	10.75	0.31	54.51	0.12	0.13	0.11	0.39	0.06	0.03	0.02	1.79	0.02	42.30	99.79	96.77	0.71	0.26
0924-2-1	White limestone	10.66	0.41	54.17	0.13	0.09	0.09	0.38	0.09	0.03	0.02	2.40	0.01	41.70	99.53	96.16	0.94	0.23
CQ13	White limestone	10.65	0.19	54.63	0.02	0.14	0.09	0.33	0.10	0.02	0.03	2.40	0.01	42.06	100.01	96.98	1.74	0.18
CQ11	Gray Pink limestone	10.57	0.26	54.48	0.11	0.13	0.10	0.35	0.12	0.03	0.04	2.26	0.01	42.04	99.94	96.71	1.33	0.25
0924-1-2	Pink limestone	10.53	0.51	53.47	0.21	0.14	0.15	0.37	0.05	0.04	0.03	3.04	0.02	41.51	99.54	94.92	1.23	0.36
CQ10	Pink limestone	10.52	0.27	52.81	0.15	0.13	0.12	0.32	0.07	0.02	0.03	4.39	0.02	41.31	99.65	93.75	3.42	0.29
CQ9	Light gray limestone	10.43	0.22	54.62	0.11	0.10	0.09	0.36	0.08	0.02	0.02	2.47	0.01	41.89	99.99	96.96	1.68	0.22
CQ8	White limestone	10.38	0.31	54.26	0.08	0.14	0.10	0.39	0.08	0.03	0.03	2.22	0.01	42.18	99.83	96.32	1.13	0.24
0924-1-1	White limestone	10.37	0.28	54.77	0.08	0.10	0.09	0.34	0.08	0.02	0.02	2.28	0.02	41.91	99.99	97.22	1.28	0.19
CQ5	White limestone	10.22	0.65	52.21	0.14	0.13	0.15	0.38	0.07	0.03	0.03	4.92	0.02	40.97	99.69	92.67	2.64	0.28
CQ4	White limestone	10.12	0.38	53.19	0.17	0.08	0.13	0.35	0.07	0.03	0.03	4.12	0.02	41.34	99.90	94.41	2.79	0.26
CQ3	White limestone	10.08	0.62	52.23	0.08	0.20	0.16	0.37	0.06	0.03	0.03	5.05	0.02	41.01	99.87	92.72	2.86	0.30
CQ2	White limestone	10.00	0.76	51.30	0.19	0.12	0.18	0.39	0.05	0.02	0.04	6.34	0.02	40.38	99.80	91.06	3.67	0.32
CQ1	White limestone	9.97	0.56	52.46	0.18	0.10	0.15	0.40	0.06	0.03	0.03	5.06	0.02	40.99	100.03	93.12	3.09	0.29

Sample	Lithology	Position	Al	V	Cr	Co	Ni	Cu	Zn	Rb	Sr	Zr	Mo	Ba	U	Th
K/T12	Dark red limestone	14.80	0.60	12.56	11.24	5.64	12.07	7.48	16.33	8.09	611.91	8.66	1.15	44.78	0.18	0.81
CO-49	Dark red limestone	13.75	0.26	4.88	6.81	2.10	3.76	4.53	11.03	4.05	585.77	3.72	0.74	120.65	0.08	0.34
CQ16	Pink limestone	10.96	0.41	3.65	7.26	1.55	3.01	6.57	20.92	3.37	465.76	3.41	0.94	489.63	0.08	0.33
CQ15	Pink limestone	10.85	0.23	2.73	6.03	1.42	2.52	6.44	44.82	2.63	519.39	2.60	0.61	1276.09	0.08	0.25
0924-2-2	Pink limestone	10.82	0.30	9.16	5.05	1.95	4.08	7.21	19.68	4.03	556.94	3.26	0.61	429.69	0.10	0.32
CQ14	Light Pink limestone	10.78	0.42	3.89	6.57	1.91	4.04	7.25	10.20	3.63	564.30	3.42	0.62	65.64	0.08	0.37
CO-37	Pink limestone	10.75	0.16	2.72	8.00	1.19	1.45	5.48	23.94	2.39	390.73	2.33	0.96	638.48		0.24
0924-2-1	White limestone	10.66	0.22	6.47	7.92	1.12	2.15	11.08	7.63	1.71	415.73	1.53	0.79	64.07	0.06	0.17
CQ13	White limestone	10.65	0.10	3.00	6.26	1.10		5.36	28.34	1.69	431.74	1.72	0.82	706.55	0.06	0.17
CQ11	Gray Pink limestone	10.57	0.14	3.52	7.37	1.69	3.60	5.32	14.54	1.93	400.12	1.70	0.86	283.49	0.06	0.16
0924-1-2	Pink limestone	10.53	0.27	4.21	4.32	2.17	3.86	6.08	12.07	3.53	553.93	2.86	0.50	82.80	0.09	0.34
CQ10	Pink limestone	10.52	0.14	6.00	5.47	1.37	1.88	5.13	20.31	2.58	462.49	2.13	0.74	490.14	0.08	0.24
CQ9	Light gray limestone	10.43	0.12	3.91	7.10	0.93	1.68	6.09	9.48	1.64	399.80	1.44	0.76	62.13	0.10	0.16
CQ8	White limestone	10.38	0.16	6.27	9.43	1.26	5.40	15.40	8.05	1.97	424.24	1.71	1.33	22.92		0.18
0924-1-1	White limestone	10.37	0.15	2.31	5.22	1.12		3.34	23.01	1.88	428.60	1.96	0.57	582.72	0.06	0.19
CQ5	White limestone	10.22	0.34	10.50	6.21	1.31	1.74	28.17	11.51	3.98	528.22	3.48	0.61	139.74	0.23	0.35
CQ4	White limestone	10.12	0.20	5.85	10.05	1.24	3.29	13.25	14.82	3.24	535.29	3.06	1.06	41.31	0.12	0.32
CQ3	White limestone	10.08	0.33	6.48	12.30	1.36	2.99	13.06	16.78	4.39	569.68	3.83	0.99	158.43	0.12	0.36
CQ2	White limestone	10.00	0.40	6.33	9.65	1.61	7.92	27.25	18.50	4.68	537.41	3.92	0.93	38.69	0.11	0.39
CQ1	White limestone	9.97	0.30	5.04	12.86	1.40	11.09	21.32	12.64	3.64	464.80	3.35	2.60	161.23	0.09	0.32

Sample	Lithology	Position	La	Ce	Pr	Nd	Sm	Eu	Gd	Tb	Dy	Ho	Er	Tm	Yb	Lu	∑REE	_Ce	_Eu
K/T12	Dark red limestone	14.80	11.96	9.33	2.12	9.02	1.66	0.39	1.87	0.25	1.74	0.41	1.15	0.16	0.96	0.14	41.17	0.42	1.03
CO-49	Dark red limestone	13.75	7.54	4.52	1.04	4.29	0.76	0.20	0.96	0.12	0.89	0.22	0.67	0.09	0.55	0.08	21.92	0.36	1.06
CQ16	Pink limestone	10.96	7.05	3.87	0.89	3.84	0.67	0.18	0.89	0.11	0.84	0.22	0.64	0.09	0.54	0.08	19.93	0.34	1.09
CQ15	Pink limestone	10.85	7.26	4.09	0.91	3.75	0.64	0.25	0.97	0.11	0.84	0.22	0.66	0.10	0.58	0.09	20.46	0.35	1.42
0924-2-2	Pink limestone	10.82	8.49	4.65	1.15	4.87	0.85	0.23	1.18	0.15	1.08	0.26	0.76	0.11	0.63	0.10	24.52	0.33	1.05
CQ14	Light Pink limestone	10.78	8.50	5.20	1.17	4.81	0.89	0.21	1.11	0.14	1.03	0.25	0.74	0.11	0.65	0.10	24.92	0.37	0.98
CO-37	Pink limestone	10.75	6.18	3.30	0.75	3.08	0.54	0.17	0.77	0.10	0.74	0.19	0.56	0.08	0.49	0.08	17.02	0.34	1.18
0924-2-1	White limestone	10.66	6.90	3.03	0.79	3.32	0.54	0.15	0.75	0.10	0.76	0.20	0.63	0.09	0.54	0.09	17.87	0.28	1.08
CQ13	White limestone	10.65	4.85	2.50	0.55	2.35	0.40	0.15	0.57	0.08	0.54	0.14	0.44	0.06	0.36	0.06	13.06	0.33	1.39
CQ11	Gray Pink limestone	10.57	6.61	3.32	0.78	3.32	0.57	0.15	0.78	0.10	0.78	0.20	0.63	0.08	0.56	0.09	17.97	0.32	1.05
0924-1-2	Pink limestone	10.53	9.21	5.77	1.27	5.22	1.01	0.24	1.14	0.15	1.10	0.27	0.81	0.12	0.70	0.11	27.11	0.38	1.05
CQ10	Pink limestone	10.52	7.44	3.61	0.95	4.06	0.71	0.21	0.98	0.12	0.96	0.22	0.69	0.10	0.56	0.08	20.69	0.30	1.14
CQ9	Light gray limestone	10.43	5.58	2.56	0.66	2.72	0.45	0.12	0.66	0.08	0.68	0.18	0.50	0.07	0.43	0.06	14.74	0.29	0.97
CQ8	White limestone	10.38	6.47	2.80	0.71	3.00	0.48	0.13	0.72	0.10	0.76	0.19	0.60	0.08	0.53	0.08	16.66	0.28	1.02
0924-1-1	White limestone	10.37	5.01	2.67	0.60	2.41	0.43	0.14	0.60	0.07	0.59	0.15	0.43	0.06	0.40	0.06	13.63	0.34	1.22
CQ5	White limestone	10.22	8.37	4.72	1.11	4.59	0.83	0.21	1.11	0.13	1.07	0.25	0.74	0.10	0.65	0.10	24.00	0.34	1.00
CQ4	White limestone	10.12	6.50	3.49	0.81	3.39	0.61	0.15	0.81	0.10	0.76	0.20	0.60	0.08	0.49	0.08	18.06	0.33	0.96
CQ3	White limestone	10.08	8.02	4.41	1.06	4.40	0.78	0.19	1.05	0.13	0.99	0.25	0.73	0.10	0.63	0.10	22.84	0.34	0.95
CQ2	White limestone	10.00	8.33	4.83	1.14	4.63	0.82	0.20	1.08	0.14	1.03	0.25	0.80	0.10	0.64	0.10	24.08	0.35	0.98
CQ1	White limestone	9.97	6.58	3.89	0.87	3.61	0.64	0.16	0.85	0.10	0.79	0.21	0.63	0.08	0.53	0.09	19.02	0.36	1.00

All oxides and bulk parameters are reported as %, minor elements and trace elements are reported in μg/g.